Effects of surface-bulk hybridization in three-dimensional topological metals

Yi-Ting Hsu,[1,*] Mark H. Fischer,[1,2] Taylor L. Hughes,[3] Kyungwha Park,[4] and Eun-Ah Kim[1]
[1]*Department of Physics, Cornell University, Ithaca, New York 14853, USA*
[2]*Department of Condensed Matter Physics, Weizmann Institute of Science, Rehovot 76100, Israel*
[3]*Department of Physics, University of Illinois, 1110 West Green Street, Urbana, Illinois 61801, USA*
[4]*Department of Physics, Virginia Tech, Blacksburg, Virginia 24061, USA*
(Received 14 January 2014; published 29 May 2014)

Identifying the effects of surface-bulk coupling is a key challenge in exploiting the topological nature of the surface states in many available three-dimensional topological "metals." Here we combine an effective-model calculation and an *ab initio* slab calculation to study the effects of the lowest order surface-bulk interaction: hybridization. In the effective-model study, we discretize an established low-energy effective four-band model and introduce hybridization between surface bands and bulk bands in the spirit of the Fano model. We find that hybridization enhances the energy gap between bulk and Dirac surface states and preserves the latter's spin texture qualitatively, albeit with a reduced spin-polarization magnitude. Our *ab initio* study finds the energy gap between the bulk and the surface states to grow upon an increase in the slab thickness, very much in qualitative agreement with the effective-model study. Comparing the results of our two approaches, we deduce that the experimentally observed low magnitude of the spin polarization can be attributed to a hybridization-type surface-bulk interaction. We discuss evidence for such hybridization in existing ARPES data.

DOI: 10.1103/PhysRevB.89.205438 PACS number(s): 73.20.At

I. INTRODUCTION

Many discrepancies between experimental measurements and theoretical predictions of ideal topological insulators (TIs) are attributed to the fact that the chemical potential lies in the conduction band and the bulk band interferes with measurements [1–4]. That is, many available TI materials are actually metallic. Recent developments in thin-film experiments [4–8] further call for studies of surface-bulk (S-B) electron interaction in films. However, explicit first-principles calculations on TI films are limited to very thin slabs, with a thickness less than 10 nm due to the computational cost. Therefore, there is a need for a simple microscopic model which incorporates S-B interactions that can be used to study how physical properties depend on the film thickness.

One important question such a model should address is the effect of S-B interaction on the spin texture. The surface spin texture is a key physical characteristic of topological surface states in ideal TIs. While low-energy effective theories guided by symmetries predict perfect spin-momentum locking for topological surface states within the bulk gap, spin- and angle-resolved photoemission spectroscopy (SARPES) data show lower in-plane spin polarization and total spin magnitude [9–11]. On the other hand, an *ab initio* calculation on a few-quintuple-layer (QL) slab [11] found both the spin polarization and the total spin magnitude to be much smaller. Although reductions in spin polarization and total spin magnitude are to be anticipated at large surface Fermi momenta where hexagonal warping manifests [12–14], little is understood about the reduction observed at small Fermi momenta and how the S-B interaction affects the spin texture. However, such understanding is crucial for pursuing technical applications of spin-momentum locking in thin films of TIs in the metallic regime [15–17].

Our starting point is the observation made by [18] that the lowest order electron-electron interaction term between the surface state and the bulk states can be viewed as a hybridization term in the Fano model [19]. The key effect of hybridization in this low-energy effective theory is to spectroscopically separate surface states localized on the surface from the extended metallic bands. Building on the principles underlying this low-energy effective theory, we study hybridization effects with a microscopic model of three-dimensional (3D) time-reversal-invariant strong TIs to address the thickness dependence of physical quantities and connect the results to *ab initio* slab calculations. Specifically, we study TI slabs of finite thickness in the presence of S-B interaction from two complementary perspectives: a simple microscopic model including the lowest order S-B interaction and an *ab initio* calculation of a few-QL Bi_2Se_3. We focus on how the spectroscopic properties and the spin texture evolve as a function of the film thickness.

The paper is structured as follows. In Sec. II we construct a lattice model for a slab with S-B hybridization and study the spectroscopic properties of the model as well as the effects of S-B hybridization on the spin texture. In Section III we present an *ab initio* study on 4,5,6-QL Bi_2Se_3 using density functional theory (DFT) and discuss the insight the simple hybridization model offers in understanding the *ab initio* results. We then conclude in Sec. IV with a discussion of the implications of our results and open questions.

II. LATTICE MODEL FOR A SLAB WITH S-B HYBRIDIZATION

A. The model

In order to introduce S-B hybridization as a perturbation in the spirit of the Fano model [18] and study its effects on a slab of finite thickness, we first need a lattice model for a slab. For this, we discretize [20] the effective continuum

*yh436@cornell.edu

model of [21], which is a four-band $\mathbf{k}\cdot\mathbf{p}$ Hamiltonian guided by symmetries and first-principle calculation results. We then make the system size finite along the vertical axis, i.e., the film growth direction.

The low-energy effective four-band model in Ref. [21] describes a strong 3D TI with a rhombohedral crystal structure such as Bi_2Se_3. In this effective model each QL is treated as a layer since the inter-QL coupling is weak, and the four lowest lying spin-orbital bands come from the mixing of the two P_z atomic orbitals from Bi and Se, referred to as P_1 and P_2, and the two spins, $\uparrow$ and $\downarrow$. We take this effective model written in terms of 4×4 Γ matrices and discretize it following the discretization scheme used for 2D TIs in Ref. [22] such that the lattice Hamiltonian reduces to the low-energy effective $\mathbf{k}\cdot\mathbf{p}$ Hamiltonian in Ref. [21] in the limit $|\mathbf{k}|\to 0$. The resulting lattice model in the rotated spin-orbital basis $\{|P_1,\uparrow\rangle, -i|P_2,\uparrow\rangle, |P_1,\downarrow\rangle, i|P_2,\downarrow\rangle\}$ is

$$H_0=\sum_{\mathbf{k}_\parallel,k_z} h_0(\mathbf{k}_\parallel,k_z)c^\dagger_{\mathbf{k}_\parallel,k_z}c_{\mathbf{k}_\parallel,k_z}, \tag{1}$$

where $c^\dagger_{\mathbf{k}_\parallel,k_z}$ is an operator creating a four-spinor in the rotated spin-orbital basis with an in-plane momentum $\mathbf{k}_\parallel=(k_x,k_y)$ and perpendicular momentum k_z, and the lattice Hamiltonian [23] is

$$\begin{aligned} h_0(\mathbf{k}_\parallel,k_z)=\epsilon_1(\mathbf{k}_\parallel,k_z)\mathbb{I}_{4\times4}+\frac{A_1}{a_z}\sin(k_za_z)\Gamma^1 \\ +\frac{A_2}{a_x}\sin(k_xa_x)\Gamma^3+\frac{A_2}{a_y}\sin(k_ya_y)\Gamma^4 \\ +M_1(\mathbf{k}_\parallel,k_z)\Gamma^5, \end{aligned} \tag{2}$$

with

$$\begin{aligned} \epsilon_1(\mathbf{k}_\parallel,k_z)\equiv C+\frac{2D_1}{a_z^2}[1-\cos(k_za_z)]+\frac{2D_2}{a_x^2}[1-\cos(k_xa_x)] \\ +\frac{2D_2}{a_y^2}[1-\cos(k_ya_y)], \end{aligned} \tag{3}$$

$$\begin{aligned} M_1(\mathbf{k}_\parallel,k_z)\equiv m-\frac{2B_1}{a_z^2}[1-\cos(k_za_z)]-\frac{2B_2}{a_x^2}[1-\cos(k_xa_x)] \\ -\frac{2B_2}{a_y^2}[1-\cos(k_ya_y)]. \end{aligned} \tag{4}$$

The Γ matrices are defined as $\Gamma^1=\sigma^z\otimes\tau^x$, $\Gamma^2=-\mathbb{I}_{2\times2}\otimes\tau^y$, $\Gamma^3=\sigma^x\otimes\tau^x$, $\Gamma^4=\sigma^y\otimes\tau^x$, and $\Gamma^5=\mathbb{I}_{2\times2}\otimes\tau^z$, where σ^j and τ^j are Pauli matrices acting on $(\uparrow,\downarrow)$ and (P_1,P_2) spaces, respectively. a_x, a_y, and a_z are the lattice constants in the x, y, and z directions, respectively. We use the parameters for Bi_2Se_3 obtained by fitting the continuum model to *ab initio* calculations [21]: $m=0.28$ eV, $A_1=2.2$ eV Å, $A_2=4.1$ eV Å, $B_1=10$ eV Å^2, $B_2=56.6$ eV Å^2, $C=-0.0068$ eV, $D_1=1.3$ eV Å^2, and $D_2=19.6$ eV Å^2.

We model a slab of Bi_2Se_3 by imposing open boundary conditions at the top and the bottom surfaces which break the translational symmetry along the z axis. Since k_z is no longer a good quantum number, while $\mathbf{k}_\parallel$ still is, we substitute $c_{\mathbf{k}_\parallel,k_z}=\frac{1}{\sqrt{N}}\sum_j e^{ik_zja_z}c_{\mathbf{k}_\parallel,j}$ in Eq. (1) and label the four-spinor operators by the in-plane momentum $\mathbf{k}_\parallel=(k_x,k_y)$ and the index of layers j stacking in the z direction. Now the Hamiltonian for a slab with N layers is

$$H_0(N)=\sum_{\mathbf{k}_\parallel}H_0(\mathbf{k}_\parallel,N), \tag{5}$$

where

$$H_0(\mathbf{k}_\parallel,N)=\sum_{j=1}^{N}\mathbb{M}c^\dagger_{\mathbf{k}_\parallel,j}c_{\mathbf{k}_\parallel,j}+\mathbb{T}c^\dagger_{\mathbf{k}_\parallel,j+1}c_{\mathbf{k}_\parallel,j}+\mathbb{T}^\dagger c^\dagger_{\mathbf{k}_\parallel,j}c_{\mathbf{k}_\parallel,j+1} \tag{6}$$

and the 4×4 matrices $\mathbb{T}$ and $\mathbb{M}$ are defined as

$$\mathbb{T}\equiv-\frac{D_1}{a_z^2}\mathbb{I}_{4\times4}+\frac{B_1}{a_z^2}\Gamma^5-\frac{iA_1}{2a_z}\Gamma^1 \tag{7}$$

and

$$\begin{aligned} \mathbb{M}\equiv\epsilon_2(\mathbf{k}_\parallel)\mathbb{I}_{4\times4}+\frac{A_2}{a_x}\sin(k_xa_x)\Gamma^3+\frac{A_2}{a_y}\sin(k_ya_y)\Gamma^4 \\ +M_2(\mathbf{k}_\parallel)\Gamma^5, \end{aligned} \tag{8}$$

where

$$\begin{aligned} \epsilon_2(\mathbf{k}_\parallel)\equiv C+\frac{2D_1}{a_z^2}+\frac{2D_2}{a_x^2}[1-\cos(k_xa_x)] \\ +\frac{2D_2}{a_y^2}[1-\cos(k_ya_y)] \end{aligned} \tag{9}$$

and

$$\begin{aligned} M_2(\mathbf{k}_\parallel)\equiv m-\frac{2B_1}{a_z^2}-\frac{2B_2}{a_x^2}[1-\cos(k_xa_x)] \\ -\frac{2B_2}{a_y^2}[1-\cos(k_ya_y)]. \end{aligned} \tag{10}$$

For the sake of simplicity, the results presented in the remainder of this section are calculated with $a_x=a_y=a_z=1$ Å.

We can diagonalize $H_0(\mathbf{k}_\parallel,N)$ as

$$\begin{aligned} H_0(\mathbf{k}_\parallel,N)=\sum_{\alpha=1}^{4N-4}E^0_{B,\alpha}(\mathbf{k}_\parallel)b^{0\dagger}_{\alpha,\mathbf{k}_\parallel}b^0_{\alpha,\mathbf{k}_\parallel} \\ +\sum_{\beta=1}^{4}E^0_{D,\beta}(\mathbf{k}_\parallel)d^{0\dagger}_{\beta,\mathbf{k}_\parallel}d^0_{\beta,\mathbf{k}_\parallel}, \end{aligned} \tag{11}$$

where $b^0_{\alpha,\mathbf{k}_\parallel}$ and $d^0_{\beta,\mathbf{k}_\parallel}$ are four-spinor annihilation operators for bulk and surface states (henceforth referred to as the "Dirac" states), respectively, in the absence of hybridization, $E^0_{B,\alpha}$ and $E^0_{D,\beta}$ are their corresponding eigenenergies. Here, α and β label the unhybridized bulk and Dirac states, respectively. All energy eigenstates are twofold degenerate as required by inversion (P) and time-reversal (T) symmetries. For each in-plane momentum $\mathbf{k}_\parallel$, four energy eigenstates with their energies closest to the Dirac point are labeled as valence ($\beta=1,2$) and conduction ($\beta=3,4$) Dirac states. α labels the remaining $4N-4$ bulk states. A natural choice for the labeling is to let $\alpha=1,\ldots,2N-2$ denote valence bulk states and let $\alpha=2N-1,\ldots,4N-4$ denote conduction bulk states, with the eigenenergies increasing monotonically with α. As the

model is derived from a low-energy effective model near the Dirac point, it will break down at high energies. However, we expect qualitatively correct results when it comes to trends of physical properties over the hybridization strength and film thickness, which only require knowledge of the low-energy physics near the insulating gap.

Now we introduce the S-B hybridization term that is allowed by symmetries in the spirit of the Fano model [19]. The Fano model is a generic model describing the mixing between extended states c_k with energy ϵ_k and a localized state b with energy ϵ through the Hamiltonian $H_F = \epsilon b^\dagger b + \sum_k [\epsilon_k c_k^\dagger c_k + A_k (c_k^\dagger b + b^\dagger c_k)]$, where A_k represents the scattering strength. [18] pointed out that H_F can be used to describe the lowest order interaction between a helical surface state and a metallic bulk band, i.e., hybridization. They studied the effects of hybridization in a field theoretic approach. Here we use a symmetry-preserving form of the S-B hybridization term in the spirit of H_F for the microscopic model of Bi_2Se_3 shown in Eq. (11) to study the effects of mixing between Dirac states and bulk states.

For simplicity, we consider the case where the hybridization strength preserves in-plane momenta $\mathbf{k}_\parallel$ and is independent of energy and $\mathbf{k}_\parallel$, i.e.,

$$h'(\mathbf{k}_\parallel) = \sum_{\alpha,\beta} g\, b^{0\dagger}_{\alpha,\mathbf{k}_\parallel} d^0_{\beta,\mathbf{k}_\parallel} + \text{H.c.} \tag{12}$$

We then impose T and P symmetries on the full hybridization perturbation $H'(\mathbf{k}_\parallel)$ by constructing $H'(\mathbf{k}_\parallel)$ through

$$H'(\mathbf{k}_\parallel) = h'(\mathbf{k}_\parallel) + Ph'(\mathbf{k}_\parallel)P^\dagger + Th'(\mathbf{k}_\parallel)T^\dagger + PTh'(\mathbf{k}_\parallel)(PT)^\dagger, \tag{13}$$

where the representations for T and P symmetry operators with the spatial inversion center at the middle point of the slab in the current $4N$ tight-binding spin-orbital basis are $T = K\, i\sigma^y \otimes \mathbb{I}_{2\times2} \otimes \mathbb{I}_{N\times N}$ with $\mathbf{k}_\parallel \leftrightarrow -\mathbf{k}_\parallel$ and $P = \mathbb{I}_{2\times2} \otimes \tau^z$ with $z : [0, N/2] \leftrightarrow [N/2, N]$ and $\mathbf{k}_\parallel \leftrightarrow -\mathbf{k}_\parallel$, respectively. Here, K is the usual complex conjugation operator. Finally, the full Hamiltonian including hybridization at a given in-plane momentum $\mathbf{k}_\parallel$ reads

$$H(\mathbf{k}_\parallel) = H_0(\mathbf{k}_\parallel, N) + H'(\mathbf{k}_\parallel). \tag{14}$$

After diagonalizing the full Hamiltonian in the tight-binding spin-orbital bases, we can write

$$H(\mathbf{k}_\parallel) = \sum_{\alpha=1}^{4N-4} E_{B,\alpha}(\mathbf{k}_\parallel) b^\dagger_{\alpha,\mathbf{k}_\parallel} b_{\alpha,\mathbf{k}_\parallel} + \sum_{\beta=1}^{4} E_{D,\beta}(\mathbf{k}_\parallel) d^\dagger_{\beta,\mathbf{k}_\parallel} d_{\beta,\mathbf{k}_\parallel}, \tag{15}$$

where $b_{\alpha,\mathbf{k}_\parallel}$, $d_{\beta,\mathbf{k}_\parallel}$, $E_{B,\alpha}$, and $E_{D,\beta}$ are defined similarly to the corresponding symbols with a superscript 0 in Eq. (11) but in the presence of hybridization. $E_{B,\alpha}$ and $E_{D,\beta}$ are again twofold degenerate, as $H(\mathbf{k}_\parallel)$ preserves the parity and time-reversal symmetries by design. α and β label the bulk and Dirac states for $H(\mathbf{k}_\parallel)$, where the terms bulk and Dirac states are defined in the same fashion as for $H_0(\mathbf{k}_\parallel, N)$ in the absence of hybridization.

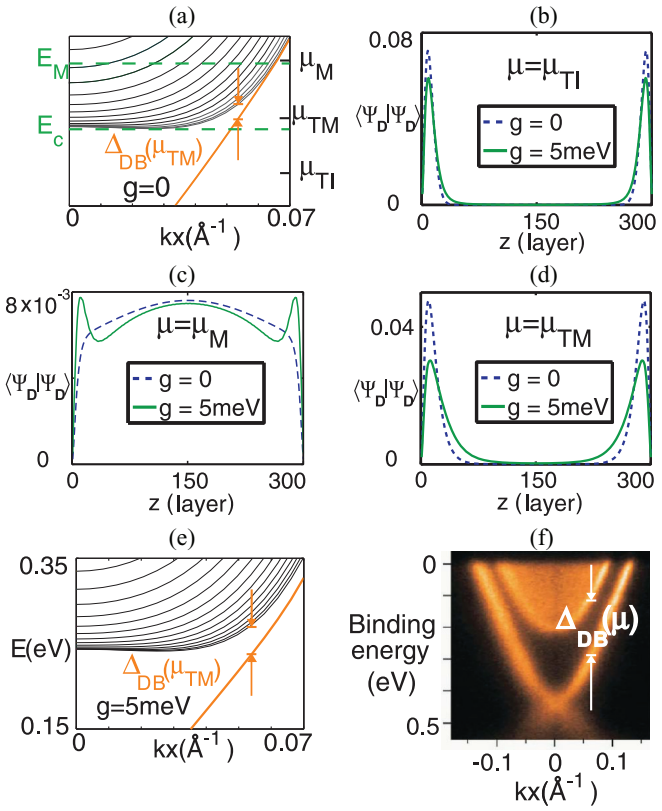

FIG. 1. (Color online) (a) Spectra of the model on a 300-layer-thick slab. The three chemical potentials $\mu_{\rm TI}$, $\mu_{\rm TM}$, and $\mu_{\rm M}$ are taken as representative points for the three regimes TI ($\mu \leqslant E_c$), M ($\mu \gtrsim E_{\rm M}$), and TM ($E_c \leqslant \mu \lesssim E_{\rm M}$) as defined in the text, respectively. (b–d) The corresponding unhybridized [dashed (blue) curve] and hybridized [solid (green) curve] spatial profiles of the pair of degenerate conduction Dirac states $|\Psi_{D,\mathbf{k}_\parallel}(z)|^2$ at $\mathbf{k}_\parallel = \mathbf{k}_{\parallel,\mu}$ with $\mu = \mu_{\rm TI}$, $\mu_{\rm TM}$, and $\mu_{\rm M}$, respectively. (e) Effect of hybridization on the spectra. (f) ARPES data on Bi_2Se_3 [3].

B. Topological metal regime

We begin our numerical study with no hybridization. In the absence of hybridization, depending on the chemical potential μ, we now define three regimes: topological insulator (TI), metal (M), and topological metal (TM) [see Fig. 1(a)]. The familiar TI regime is where the chemical potential lies within the bulk gap and the system is actually a bulk band insulator, i.e., $E_v \leqslant \mu \leqslant E_c$, with E_c being the bottom of the conduction band and E_v the top of the valence band. Within the TI regime, the Dirac states feature Rashba-type spin-momentum locking and a spatial profile localized on the surfaces. Of particular interest to us is the distinction we draw between the M and the TM regimes based on whether the Dirac states retain the spin-momentum locking and the surface localization when away from the TI regime.

In order to examine the above two properties of Dirac states, we define $|\psi_{D,\mathbf{k}_\parallel}\rangle \equiv d^\dagger_{3,\mathbf{k}_\parallel}|0\rangle$ ($d^{0\dagger}_{3,\mathbf{k}_\parallel}|0\rangle$) and $|\tilde{\psi}_{D,\mathbf{k}_\parallel}\rangle \equiv d^\dagger_{4,\mathbf{k}_\parallel}|0\rangle$ ($d^{0\dagger}_{4,\mathbf{k}_\parallel}|0\rangle$) in the presence (absence) of hybridization to represent the pair of degenerate Dirac states above the Dirac point. Now the spatial profile of the conduction Dirac states is $|\Psi_{D,\mathbf{k}_\parallel}(z)|^2 \equiv |\psi_{D,\mathbf{k}_\parallel}(z)|^2 + |\tilde{\psi}_{D,\mathbf{k}_\parallel}(z)|^2$, which is a function

of z measured from the bottom of the slab along the finite dimension of the slab. This quantity will show whether or not the Dirac states are localized on the surfaces. Let us identify a particular $\mathbf{k}_\parallel$ of interest for a given value of chemical potential as the in-plane momentum at which the chemical potential μ intersects the Dirac branch; we denote this in-plane momentum $\mathbf{k}_{\parallel,\mu}$. To illustrate the features defining the three regimes, we now report the spatial profiles and the spin polarizations of the Dirac states in the three regimes in the absence of hybridization. In the next section we add hybridization and examine its effects.

Inspecting $|\Psi_{D,\mathbf{k}_\parallel}(z)|^2$ at $\mathbf{k}_\parallel = \mathbf{k}_{\parallel,\mu}$ at the representative values of chemical potential for the three regimes $\mu_{\rm TI}$, $\mu_{\rm M}$, and $\mu_{\rm TM}$ shown in Fig. 1, we find that the spatial profile of the Dirac states $|\Psi_{D,\mathbf{k}_\parallel}(z)|^2$ indicates surface localized states of the slab in the TI regime as expected [see Fig. 1(b)]. On the other hand, in the M regime, where the chemical potential is well within the bulk conduction band, $|\Psi_{D,\mathbf{k}_\parallel}(z)|^2$ is fully delocalized over the entire slab [see Fig. 1(c)]. In this regime, the system cannot be distinguished from an ordinary M. However, even with $\mu > E_c$ there is an energy window between E_c and a crossover energy scale $E_{\rm M}$, where the Dirac states are still spatially localized on the surfaces in the sense that $|\Psi_{D,\mathbf{k}_\parallel}(z)|^2$ is peaked on each surface of the slab and decays away from the surfaces [see Fig. 1(d)]. The crossover energy scale $E_{\rm M}$ is a threshold energy, where, within the regime $\mu \gtrsim E_{\rm M}$ (regime M), wave functions for all states at in-plane momentum $\mathbf{k}_{\parallel,\mu}$ delocalize. We define the system to behave as a TM when the chemical potential lies within this window, i.e., $E_c < \mu < E_{\rm M}$, represented by $\mu_{\rm TM}$.

A detectable characteristic of TI and TM regimes is the spin-momentum locking. One measure to quantify spin-momentum locking at the surface is through the so-called "spin polarization," which is the expectation value of the spin component perpendicular to the in-plane momentum of a Dirac state, i.e.,

$$\langle S_{\hat{\mathbf{n}}}\rangle(\mathbf{k}_\parallel) \equiv \langle \psi_{D,\mathbf{k}_\parallel}|S_{\hat{\mathbf{n}}}|\psi_{D,\mathbf{k}_\parallel}\rangle \tag{16}$$

with $\hat{\mathbf{n}}\cdot\mathbf{k}_\parallel = 0$. Here the $\hat{\mathbf{n}}$ component of the quantum spin operator is defined as $S_{\hat{\mathbf{n}}} \equiv \frac{\hbar}{2}\vec{\sigma}\cdot\hat{\mathbf{n}}\otimes\mathbb{I}_{2\rm x2}\otimes\mathbb{I}_{\rm NxN}$, where $\vec{\sigma} = (\sigma_x,\sigma_y,\sigma_z)$ are Pauli matrices acting on spin, $\mathbb{I}_{2\times2}$ acts on the orbital degree of freedom, and $\mathbb{I}_{\rm N\times N}$ acts on the layer index. $\langle S_y\rangle(k_x\hat{x})$ is evaluated at $k_x\hat{x} = k_{x,\mu}\hat{x}$ and shown for $\mu = \mu_{\rm TI}$, $\mu_{\rm TM}$, and $\mu_{\rm M}$ in Fig. 2(a). We see here that, in the absence of hybridization ($g = 0$), the spin polarization stays maximal in the TI and TM regimes while rapidly dropping upon entering the M regime. Another quantity of experimental interest is the total spin magnitude associated with the Dirac states with in-plane momentum $\mathbf{k}_\parallel$ defined in terms of spin polarization as

$$S(\mathbf{k}_\parallel) \equiv \sqrt{\sum_{i=x,y,z}[\langle S_i\rangle(\mathbf{k}_\parallel)]^2}. \tag{17}$$

Figures 2(a) and 2(b) show that the spin-momentum locking quantified using these measures clearly distinguishes the TM regime from the ordinary M regime in the absence of hybridization.

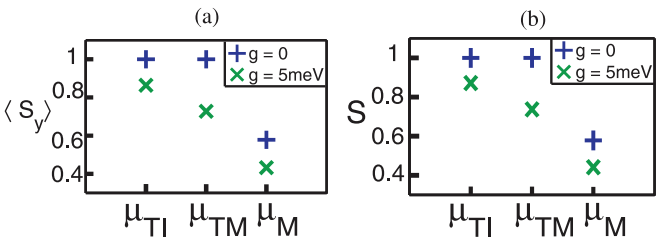

FIG. 2. (Color online) The effect of hybridization on the degree of spin-momentum locking in different regimes. Spin expectation values are calculated for a 300-layer-thick slab using a conduction Dirac state $|\psi_{D,k_x\hat{x}}\rangle$ with $k_x = k_{x,\mu}$ at different representative chemical potentials $\mu = \mu_{\rm TI}$, $\mu_{\rm TM}$, and $\mu_{\rm M}$. (a) Spin polarization $\langle S_y\rangle(k_x\hat{x})$. (b) Total spin magnitude $S(k_x\hat{x})$ (defined in the text).

C. Effects of S-B hybridization

We now turn to the effects of hybridization. One effect of hybridization that is manifest in the experimental detection of Dirac surface states in the TM regime is an increase in the bulk-Dirac-state energy gap. We quantify this energy gap, for a given chemical potential μ, using the energy difference between a Dirac state above the Dirac point and the energetically closest bulk state, defined by

$$\Delta_{DB}(\mu) \equiv E^{(0)}_{B,2N-1}(k_{\parallel,\mu}) - E^{(0)}_{D,3}(k_{\parallel,\mu}), \tag{18}$$

in the presence (absence) of hybridization. Comparing Figs. 1(a) to 1(e), we find that the key effect of hybridization that is spectroscopically detectable is the increase in $\Delta_{DB}(\mu)$ in both the TM and the M regimes compared to the TI regime. Otherwise the spectra in the absence or presence of hybridization look similar. Note that most ARPES data on 3D TIs exhibit a clear energy gap between the Dirac branch and the bulk states at a chemical potential well into the bulk band as shown in Fig. 1(f). This experimental trend hints at the possibility that a sizable hybridization between Dirac states and the bulk states is common in 3D TI materials. In order to demonstrate the effect of hybridization, we choose the value of $g = 5$ meV, which is subdominant to all the hopping terms yet substantial in this paper. However, key effects of hybridization do not depend qualitatively on the value of g.

Another effect of hybridization is to broaden the Dirac state wave functions in the TI and TM regimes. The degree of broadening depends on the chemical potential μ, hybridization strength g, and slab thickness N. However, as long as g is the smallest energy scale in the total Hamiltonian, as is the case for Figs. 1(b)–1(d), the Dirac states in the TI and TM regimes remain localized on the surfaces. A tangible consequence of the wave-function broadening is the quantitative suppression of the spin-momentum locking. As mentioned earlier, in the absence of hybridization the Dirac states of TI and TM exhibit a maximal degree of spin-momentum locking. However, hybridization rotates the spin vectors of different atomic orbitals and layers away from the direction perpendicular to the in-plane momentum. Hence, both measures of spin-momentum locking shown in Fig. 2 show a quantitative reduction upon hybridization. This is in qualitative agreement with the low values of spin polarization and total spin magnitude found in a first-principles calculation of a thin slab in a previous work [11] and our DFT results in the next section. Note that the hybridization still preserves the

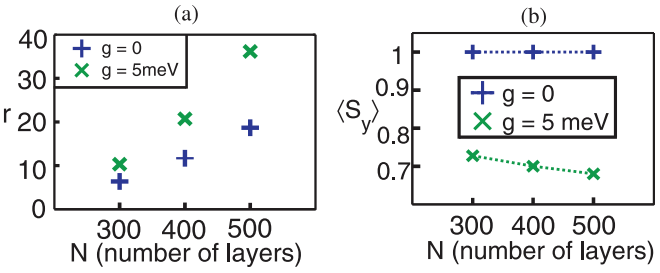

FIG. 3. (Color online) Thickness dependence of the hybridization effects. (a) Dimensionless measure of the bulk-Dirac energy gap $r = \Delta_{DB}/\Delta_{BB}$ (defined in the text) at different slab thicknesses for $\mu = \mu_{\rm TM}$. (b) Spin polarization of a conduction Dirac state $\langle S_y\rangle(k_x\hat{x})$ at $\mu = \mu_{\rm TM}$.

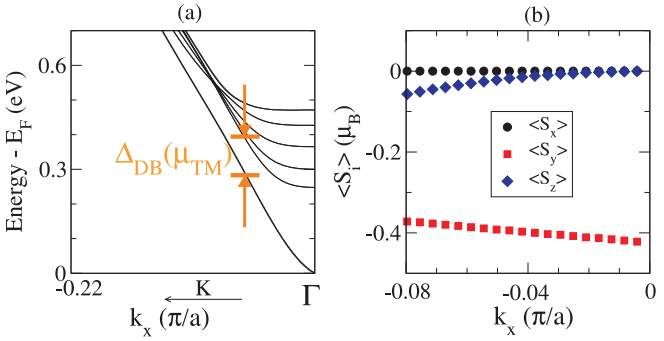

FIG. 4. (Color online) (a) DFT-calculated band structure of a 6-QL slab of Bi_2Se_3. (b) DFT-calculated spin expectation values of the conduction Dirac state $\langle S_i\rangle(k_x\hat{x})$ for a 6-QL Bi_2Se_3 slab.

spin-texture winding despite the quantitative reduction in the spin polarization.

Finally, we study how the effects of hybridization on the two experimentally accessible characteristics of the TM regime, namely, how the bulk-Dirac energy gap $\Delta_{DB}(\mu)$ and the spin polarization $\langle S_{\hat{n}}\rangle(\mathbf{k}_\parallel)$ of a Dirac state vary with the slab thickness. Since the quantized energy spacings due to finite-size effects decreases with increasing slab thickness, we consider a dimensionless measure that quantifies the bulk-Dirac energy gap:

$$r(\mu) \equiv \Delta_{DB}(\mu)/\Delta_{BB}(\mu), \tag{19}$$

where $\Delta_{BB}(\mu) \equiv E^{(0)}_{B,2N+1}(k_{\parallel,\mu}) - E^{(0)}_{B,2N-1}(k_{\parallel,\mu})$ is the energy spacing in the presence (absence) of hybridization between the two lowest lying conduction bulk branches measured at the same in-plane momentum $\mathbf{k}_{\parallel,\mu}$, where $\Delta_{DB}(\mu)$ is calculated. This dimensionless quantity $r(\mu)$ allows us to compensate for finite-size effects, though Δ_{BB} would be hard to measure experimentally for realistic bulk samples due to the lack of the required energy resolution. Figure 3(a) shows that the hybridization-induced enhancement in the bulk-Dirac energy gap becomes more prominent with increasing slab thickness. Comparing the existing ARPES data on bulk samples [3] and on thin films [5], we find the Dirac branch to be better separated from the bulk states in the bulk samples than in the thin films, which is consistent with the hybridization effect shown in Fig. 3(a). Finally Fig. 3(b) shows that the reduction in spin-polarization magnitude $|\langle S_y\rangle(k_x\hat{x})|$ is also intensified with increasing thickness. Such an enhancement in the impact of hybridization with an increase in slab thickness can be explained by the fact that a thicker slab implies a larger number of bulk states that mix with a fixed number of Dirac surface states for a given strength of hybridization g.

III. DFT CALCULATIONS OF THIN Bi_2Se_3 SLABS

Now we turn to an *ab initio* study of thin slabs to compare with the simple phenomenological model of hybridization we explored in the previous section. The approach of the previous section is limited, in the sense that it builds on a low-energy effective description of the band structure and that there is no detailed knowledge of the hybridization strength g which could, in principle, be $\mathbf{k}_\parallel$ dependent. On the other hand, the DFT approach on slabs, which does not require calculating the surface and bulk separately as in the calculations of semi-infinite systems [21], is limited to very thin films of several QLs due to computational limits. By combining the two approaches, we extract a more robust understanding of the effects of hybridization in the TM regime and the implications of their trends over film thickness.

We calculate the electronic structure of $Bi_2Se_3(111)$ slabs of 4–6 QLs using the VASP code [24,25] with the projector-augmented-wave method [26], within the generalized-gradient approximation [27]. Spin-orbit coupling is included self-consistently. We use experimental lattice constants [28] and an energy cutoff of 420 eV with a $31 \times 31 \times 1$ k-point grid. Our DFT calculations are limited up to 6 QLs. For 5–6 QLs, the overlap between the top and the bottom surface states is already very small, yielding an energy gap of the order of milli–electron volts at Γ. Expectation values of spin components $\langle S_x\rangle, \langle S_y\rangle, \langle S_z\rangle$ are calculated from the summation of the expectation values of each atom.

Figure 4 shows the DFT-calculated band structure and spin expectation values $\langle S_i\rangle(k_x\hat{x})$ of a 6-QL slab. The surface states are doubly degenerate and have a Dirac dispersion and we show five confined states in the bulk conduction band region [Fig. 4(a)]. For small $|k_x|$ values, $\langle S_y\rangle$ of a Dirac conduction state is clearly dominant over other components and exhibits spin-momentum locking [Fig. 4(b)]. As $|k_x|$ increases, a small z component of spin expectation value develops. However, over the entire range of k_x, $\langle S_y\rangle$ is much less than the maximal value, in agreement with a previous DFT study [11]. A comparison between Fig. 2 and Fig. 4(b) indicates that our hybridization model is an effective way to capture the broadening of the Dirac surface state wave function and the resulting reduction in the spin polarization and the total spin magnitude [29].

Now we discuss the thickness dependence of the bulk-Dirac energy gap measure and the spin polarization. We calculate the dimensionless measure of the bulk-Dirac energy gap $r = \Delta_{DB}/\Delta_{BB}$ in the TM regime at the $\mathbf{k}_\parallel$ point, where the Dirac surface state branch has a slightly higher energy than the bottom of the conduction band E_c, as indicated in Fig. 4(a). We find that the ratio $\Delta_{BB}(N_1)/\Delta_{BB}(N_2)$ is close to $(N_2/N_1)^2$ at the $k_\parallel$ point of interest as expected of the finite-size-effect origin of the scale $\Delta_{BB}(N)$. Surprisingly, despite the small range of thicknesses accessible to the slab DFT calculation,

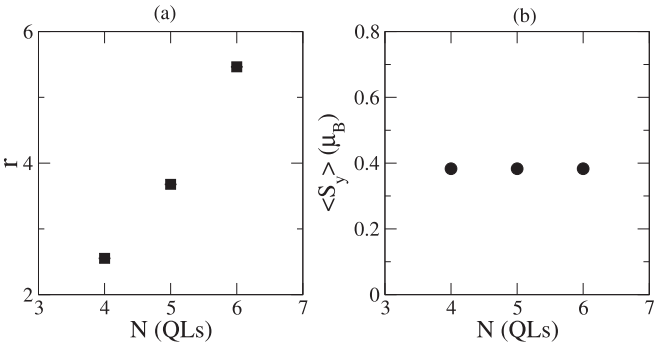

FIG. 5. (a) Ratio $r = \Delta_{DB}/\Delta_{BB}$ within the TM regime, calculated at a fixed $\mathbf{k}_\parallel$. (b) $\langle S_y \rangle$ of the conduction Dirac state calculated using DFT as a function of the slab thickness N.

the dimensionless measure of the bulk-Dirac energy gap $r = \Delta_{DB}/\Delta_{BB}$ in Fig. 5(a) shows a significant increase upon an increase in the slab thickness. This is qualitatively consistent with observations from the effective model and hybridization effects in Sec. II. On the other hand, the range of thicknesses in the present calculation appears to be too small to show any change in the $\langle S_y \rangle$ as a function of the slab thickness [Fig. 5(b)].

IV. CONCLUSION

We have combined a Fano-type hybridization model calculation with an *ab initio* slab calculation to study the lowest order effects of S-B interaction in TIs with a particular focus on the TM regime. We defined the TM regime of a TI to be where the Dirac surface states and bulk states coexist and interact yet the spin winding is preserved, albeit with a reduced spin-polarization magnitude. The hybridization model presented in Sec. II captures the spin-polarization reduction of the Dirac states originating from the hybridization with bulk states. Given the metallic behavior of most TIs and the experimental evidence of reduced spin polarization, our simple model offers a useful starting point for applications of TIs which need to take real materials in the TM regime into account. Moreover, the hybridization-driven bulk-Dirac energy gap explains why the Dirac branch shows up so well separated from bulk states in ARPES experiments. Note that this energy gap and the suppression of total spin magnitudes are both experimentally observed phenomena that cannot be accessed by the typical approach of coupling a single "surface layer" to a bulk electronic structure to include surface states in semi-infinite systems as in Ref. [21]. We propose SARPES experiments for films of varying thickness to test our predictions for hybridization-driven suppression of spin polarization for further vindication of the model.

Promising future directions include DFT tools to study slightly thicker systems. This might reveal thickness dependence on spin polarization and be compared to the results of the simple model. Also, this would reveal more detailed knowledge of the magnitude and $\mathbf{k}_\parallel$ dependence of the hybridization strength g. Preliminary DFT results show that $g(\mathbf{k}_\parallel)$ has a significant $\mathbf{k}_\parallel$ dependence. Another interesting direction will be to study consequences of the hybridization effect on transport properties. Many puzzling aspects of transport experiments [4,6–8] have been attributed to the presence of bulk states or S-B interaction. There is growing theoretical interest in the transport properties of topological edge states in the presence of metallic bulk states [30–33] as well. Our microscopic model offers a simple starting point to theoretically address effects of S-B interaction on transport in 3D TIs.

ACKNOWLEDGMENTS

We thank S. Oh for stimulating discussions. E.-A.K., Y.-T.H., and M.H.F. were supported in part by NSF Career Grant No. DMR-095582 and in part by the Cornell Center for Materials Research with funding from the NSF MRSEC program (DMR-1120296). K.P. was supported by NSF Grant Nos. DMR-0804665 and DMR-1206354 and the San Diego Supercomputer Center (DMR-060009N). T.L.H. was supported by the U.S. DOE under Grant No. QMN DE-FG02-07ER46453.

[1] S. Kim, M. Ye, K. Kuroda, Y. Yamada, E. E. Krasovskii, E. V. Chulkov, K. Miyamoto, M. Nakatake, T. Okuda, Y. Ueda, K. Shimada, H. Namatame, M. Taniguchi, and A. Kimura, Phys. Rev. Lett. **107**, 056803 (2011).

[2] S. R. Park, W. S. Jung, C. Kim, D. J. Song, C. Kim, S. Kimura, K. D. Lee, and N. Hur, Phys. Rev. B **81**, 041405 (2010).

[3] M. Bianchi, D. Guan, S. Bao, J. Mi, B. B. Iversen, P. D. King, and P. Hofmann, Nat. Commun. **1**, 128 (2010).

[4] H. Steinberg, J.-B. Laloe, V. Fatemi, J. S. Moodera, and P. Jarillo-Herrero, Phys. Rev. B **84**, 233101 (2011).

[5] Y. Zhang, K. He, C.-Z. Chang, C.-L. Song, L.-L. Wang, X. Chen, J.-F. Jia, Z. Fang, X. Dai, W.-Y. Shan, S.-Q. Shen, Q. Niu, X.-L. Qi, S.-C. Zhang, X.-C. Ma, and Q.-K. Xue, Nat. Phys. **6**, 584 (2010).

[6] N. Bansal, Y. S. Kim, M. Brahlek, E. Edrey, and S. Oh, Phys. Rev. Lett. **109**, 116804 (2012).

[7] M. Liu, C.-Z. Chang, Z. Zhang, Y. Zhang, W. Ruan, K. He, L.-l. Wang, X. Chen, J.-F. Jia, S.-C. Zhang, Q.-K. Xue, X. Ma, and Y. Wang, Phys. Rev. B **83**, 165440 (2011).

[8] Y. S. Kim, M. Brahlek, N. Bansal, E. Edrey, G. A. Kapilevich, K. Iida, M. Tanimura, Y. Horibe, S.-W. Cheong, and S. Oh, Phys. Rev. B **84**, 073109 (2011).

[9] D. Hsieh, Y. Xia, D. Qian, L. Wray, J. H. Dil, F. Meier, J. Osterwalder, L. Patthey, J. G. Checkelsky, N. P. Ong, A. V. Fedorov, H. Lin, A. Bansil, D. Grauer, Y. S. Hor, R. J. Cava, and M. Z. Hasan, Nature **460**, 1101 (2009).

[10] Z.-H. Pan, E. Vescovo, A. V. Fedorov, D. Gardner, Y. S. Lee, S. Chu, G. D. Gu, and T. Valla, Phys. Rev. Lett. **106**, 257004 (2011).

[11] O. V. Yazyev, J. E. Moore, and S. G. Louie, Phys. Rev. Lett. **105**, 266806 (2010).
[12] Y. L. Chen, J. G. Analytis, J.-H. Chu, Z. K. Liu, S.-K. Mo, X. L. Qi, H. J. Zhang, D. H. Lu, X. Dai, Z. Fang, S. C. Zhang, I. R. Fisher, Z. Hussain, and Z.-X. Shen, Science **325**, 178 (2009); http://www.sciencemag.org/content/325/5937/178.full.pdf.
[13] L. Fu, Phys. Rev. Lett. **103**, 266801 (2009).
[14] K. Kuroda, M. Arita, K. Miyamoto, M. Ye, J. Jiang, A. Kimura, E. E. Krasovskii, E. V. Chulkov, H. Iwasawa, T. Okuda, K. Shimada, Y. Ueda, H. Namatame, and M. Taniguchi, Phys. Rev. Lett. **105**, 076802 (2010).
[15] I. Garate and M. Franz, Phys. Rev. Lett. **104**, 146802 (2010).
[16] T. Yokoyama, J. Zang, and N. Nagaosa, Phys. Rev. B **81**, 241410 (2010).
[17] M. Fischer, A. Vaezi, A. Manchon, and E.-A. Kim, arXiv:1305.1328.
[18] D. L. Bergman and G. Refael, Phys. Rev. B **82**, 195417 (2010).
[19] G. D. Mahan, *Many-Particle Physics*, 3rd ed. (Plenum, New York, 2000).
[20] A similar discretization was used in other papers, e.g., G. Rosenberg and M. Franz, Phys. Rev. B **85**, 195119 (2012).
[21] H. Zhang, C.-X. Liu, X.-L. Qi, X. Dai, Z. Fang, and S.-C. Zhang, Nat. Phys. **5**, 438 (2009).
[22] M. Konig, H. Buhmann, L. W. Molenkamp, T. Hughes, C.-X. Liu, X.-L. Qi, and S.-C. Zhang, J. Phys. Soc. Jpn. **77**, 031007 (2008).
[23] The lattice Hamiltonian $h_0(\mathbf{k}_\parallel, k_z)$ does not have in-plane threefold rotational symmetry of the continuum Hamiltonian. However, we do not expect this to change any of our conclusions in a qualitative manner.
[24] G. Kresse and J. Furthmüller, Phys. Rev. B **54**, 11169 (1996).
[25] G. Kresse and J. Furthmüller, Comp. Mat. Sci. **6**, 15 (1996).
[26] P. E. Blöchl, Phys. Rev. B **50**, 17953 (1994).
[27] J. P. Perdew, K. Burke, and M. Ernzerhof, Phys. Rev. Lett. **77**, 3865 (1996).
[28] S. Nakajima, J. Phys. Chem. Solids **24**, 479 (1963).
[29] Our DFT calculations also show evidence of the hexagonal warping effect [13, 14] for $k_x \gtrsim 0.08\pi/a$.
[30] D. L. Bergman, Phys. Rev. Lett. **107**, 176801 (2011).
[31] M. Barkeshli and X.-L. Qi, Phys. Rev. Lett. **107**, 206602 (2011).
[32] A. Karch, Phys. Rev. B **83**, 245432 (2011).
[33] A. Junck, K. W. Kim, D. L. Bergman, T. Pereg-Barnea, and G. Refael, Phys. Rev. B **87**, 235114 (2013).